Low-Temperature UV-Processing of Nanocrystalline Nanoporous Thin TiO_2 Films: An Original Route toward Plastic Electrochromic Systems

Zoë Tebby,[†] Odile Babot,[†] Thierry Toupance,*[,†] Dae-Hoon Park,[‡] Guy Campet,[‡] and Marie-Hélène Delville[‡]

Institut des Sciences Moléculaires, Groupe Matériaux UMR 5255 CNRS, University of Bordeaux 1, 351 Cours de la Libération, F-33405 Talence Cedex, France, and Institut de Chimie de la Matière Condensée de Bordeaux, UPR 9048 CNRS, Château Brivazac, Avenue du Docteur A. Schweitzer, F-33608 Pessac Cedex, France

Received July 25, 2008. Revised Manuscript Received September 30, 2008

The direct UV irradiation of nanoparticulate TiO_2 films deposited by the "doctor-blade" technique led to 1.1 μm thick nanoporous and nanocrystalline anatase layers on various kinds of substrates as evidenced by various characterization techniques (MET, SEM, XRD, TGA-MS, and N_2 sorption measurements). These films demonstrated high electrochromic responses and coloration efficiencies in an ionic liquid containing a lithium salt, which is a stable and environmental friendly electrolyte. The coloration efficiency reached 38 $cm^2\ C^{-1}$ for films on ITO/plastic, for a 0.65 absorption change at 710 nm, whereas the corresponding film on FTO/glass showed a 40 $cm^2\ C^{-1}$ coloration efficiency for a 1.1 absorbance change at 710 nm. The high surface area, nanoporous texture, and nanoparticulate structure of these layers provide a large number of intercalation sites, and minimal diffusion path lengths are ensured by the high surface-to-volume ratio.

Introduction

Expanding growth of wireless technologies and modern electronics (laptops, electronic paper, mobile phones, glazing smart windows, etc.) require the design of inexpensive, lightweight, and efficient optoelectronic devices such as portable solar cells or electrochromic devices on flexible substrates. In the field of electrochromism, which is defined as a reversible change in UV−visible absorption properties of a given compound under an external electric field,[1] various chromogenic materials have been studied and developed with success. They include transition metal oxide structures such as tungsten oxide (WO_3)[2] and nickel oxide (NiO),[3] organic molecules such as viologens[4] and conductive polymers as poly(3,4-propylenedioxythiophene)[5] and hybrid systems that associate at the nanometric scale a semiconducting metal oxide and a chromogenic organic compound.[6]

Among the various binary and tertiary metal oxides available, nanocrystalline titania demonstrates several advantages for optoelectronic applications due to its nontoxic character and intrinsic physicochemical properties that combine hardness, electronic conductivity, transparency to visible light, chemical inertia and large specific surface areas. In addition, since the breakthrough performed by Grätzel et al. in 1991,[7] nanocrystalline nanoporous titanium dioxide electrodes deposited on conductive glass substrates sensitized with polypyridyl ruthenium complexes found widespread applications in the field of solar cells. The corresponding devices show energy conversion efficiencies as high as 11.2%[8] and provide a low-cost alternative to amorphous silicon photovoltaic cells. Moreover, titanium dioxide changes from white to dark blue upon lithium insertion that confers electrochromic properties to the corresponding devices. However, the usual preparation route of TiO_2 films involves high temperature sintering (above 400 °C) in order to create efficient connections between the oxide nanoparticles.[9] Such conventional routes are therefore limited to thermally stable substrates, such as glass. Consequently, several routes have been investigated to produce thick nanoporous TiO_2 electrodes at temperatures lower than 150 °C for flexible dye-sensitized solar cells such as UV irradiation of doctor-blade deposited films containing nanoparticles and a metallo-

* Corresponding author. E-mail: t.toupance@ism.u-bordeaux1.fr.
[†] University of Bordeaux 1.
[‡] Institut de Chimie de la Matière Condensée de Bordeaux.

(1) Grandqvist, C. G. *Handbook of Inorganic Electrochromic Materials*; Elsevier: Amsterdam, 1995.
(2) (a) Grandqvist, C. G. *Sol. Energy Mater. Sol. Cells.* **2000**, *60*, 201. (b) Sallard, S.; Brezesinski, T.; Smarsly, B. M. *J. Phys. Chem. C* **2007**, *111*, 7200.
(3) Boschloo, G.; Hagfeldt, A. *J. Phys. Chem. B* **2001**, *105*, 3039.
(4) Sampanthar, J. T.; Neoh, K. G.; Ng, S. W.; Kang, E. T.; Tan, K. L. *Adv. Mater.* **2000**, *12*, 1536.
(5) Welsh, D. M.; Kumar, A.; Meijer, E. W.; Reynolds, J. R. *Adv. Mater.* **1999**, *11*, 1379.
(6) (a) Cummins, D.; Boschloo, G.; Ryan, M.; Corr, D.; Rao, S. N.; Fitzmaurice, D. *J. Phys. Chem. B* **2000**, *104*, 11409. (b) Grätzel, M. *Nature* **2001**, *409*, 575. (c) Choi, S. Y.; Mamak, M.; Coombs, N.; Chopra, N.; Ozin, G. A. *Nano Lett.* **2004**, *4*, 1231.
(7) O′Regan, B.; Grätzel, M. *Nature* **1991**, *353*, 737.
(8) Nazeeruddin, Md.K.; De Angelis, F.; Fantacci, S.; Selloni, A.; Viscardi, G.; Liska, P.; Ito, S.; Takeru, B.; Grätzel, M. *J. Am. Chem. Soc.* **2005**, *127*, 16835.
(9) Lindström, H.; Södergren, S.; Solbrand, A.; Rensmo, H.; Hjelm, J.; Hagfeldt, A.; Lindquist, S-E. *J. Phys. Chem. B* **1997**, *101*, 7710.
(10) (a) Gutierrez-Tauste, D.; Zumeta, I.; Vigil, E.; Hernandez-Fenollosa, M. A.; Domenech, X.; Ayllon, J. A. *J. Photochem. Photobiol., A: Chem.* **2005**, *175*, 168. (b) Zhang, D.; Yoshida, T.; Oekermann, G.; Furuta, K.; Minoura, H. *Adv. Funct. Mater* **2006**, *16*, 1228.

10.1021/cm802030c CCC: $40.75
Published on Web 11/06/2008

organic TiO_2 precursor,[10] hydrothermal post-treatment,[11] compression,[12] chemical sintering,[13] high-frequency microwave processing,[14] or UV-laser sintering.[15]

To the best of our knowledge, only one plastic electrochromic device based on TiO_2 has been reported so far.[16] On ITO/plastic the capacity was high, but the coloration remained weak. More recently, a titania film was deposited on ITO/glass through chemical solution deposition and heated at 150 °C. The performances were a 0.27 optical density change at 550 nm and an 11 mC cm^{-2} insertion for a 0.3 μm thick film after 1 min (corresponding to a 24.5 cm^2 C^{-1} coloration efficiency (CE)).[17] It is also worthwhile to mention that a flexible nanophoto-electrochromic device on a ITO/PET substrate using a nanocrystalline TiO_2 electrode has also been described, for which the color change is not due to the TiO_2 itself but to the oxidation/reduction of methylene blue anchored on the surface of the nanoparticles.[18] The TiO_2 film is prepared by spreading a TiO_2 colloid on ITO/PET followed by a hydrothermal treatment.

In this paper, we report a preparation route of nanocrystalline nanoporous TiO_2 thin films through low-temperature processing using hydrothermal nanoparticles. Our film-manufacturing process relies on the deposition at room temperature of a TiO_2-based colloid by the "doctor-blade technique" on a conductive substrate (either a glass or plastic-based substrate). Afterward, the particle interconnection simply occurs through UV irradiation with a 125 W high pressure mercury lamp. To the best of our knowledge, such a straightforward costless method has never been reported before. The morphology and the structure of the titania thin layers have been thoroughly characterized by nitrogen adsorption/desorption porosimetry, scanning (SEM) and transmission (TEM) electron microscopies, X-ray diffraction (XRD), infrared spectroscopy (FTIR), and thermogravimetric analysis coupled to mass spectrometry (TGA-MS). As an illustrative application, the electrochromic behavior of the films coated on conductive substrates (glass and plastic) has been investigated in a lithium conductive hydrophobic ionic liquid.

There are two original aspects in our work: (i) low-temperature UV sintering of oxide nanoparticles enabling an easy process of the films on flexible substrates, which should lead to new industrial fabrication methods and applications; (ii) the use, for TiO_2, of a hydrophobic lithium conducting ionic liquid as supporting electrolyte in an electrochromic system. Indeed, such a viscous electrolyte should allow us to circumvent the low durability of the nanocrystalline titania-based optoelectronic devices due to leakage and evaporation phenomena caused by the use of organic liquid electrolytes in the most efficient systems.[19]

Experimental Section

Materials. Standard chemicals (Acros Organics, Lancaster, Aldrich) were used as received without any further purification. Lithium bis(trifluoromethylsufone)imide (LiTFSI) and 1-butyl-3-methylimidazolium (BMITFSI) were purchased from Aldrich and Solvionic, respectively. F-doped SnO_2-glass (Solems), Au/Sn-doped In_2O_3−PET and Sn-doped In_2O_3−PET (Bekaert) were used as transparent conductive substrates. Their sheet resistances, measured using a homemade four probe setup,[20] were ~10, 15, and 70 Ω/□, respectively. The conductive substrates were cleaned beforehand by sonication in propan-2-ol followed by UV irradiation in an air atmosphere.

Synthesis of the TiO_2 Nanoparticles. The preparation route of the titanium dioxide nanoparticles was adapted from the one proposed by Zaban and co-workers.[21] A solution of 19 g of tetra(propan-2-oxy)titanium (Acros Organics) in 20 mL of propan-2-ol (Acros Organics) was progressively added to 91 mg of glacial acetic acid (Lancaster) in deionized water (26.8 mL) under strong stirring (pH 3). The solution was stirred for 15 h at room temperature, and then the volatiles (acetic acid and propan-2-ol) were eliminated by heating at 120 °C. The resulting powder was then mixed with about 20 mL of deionized water and heated at 250 °C in an autoclave for 13 h. The resulting powder was dried at 300 °C for 30 min and then bleached under UV irradiation for 3 h to yield 5.3 g of titanium dioxide as a white powder (yield: 99%).

Nanocrystalline Nanoporous TiO_2 Electrode Fabrication. To prepare the porous electrodes, 0.5 g of the previous TiO_2 powder was first dispersed into 5 mL of deionized water containing pentan-2,4-dione (1 mL) and Triton X-100 (6 drops) used as a surfactant. Aliquots of the resulting colloid were deposited on the conductive substrates and spread over with a glass rod. Two parallel strips of 40 μm spacers (Magic Tape, 3M) located along the substrate edges enabled to control the thickness of TiO_2 layers and provided uncoated areas for electrical contacts.

After being dried in air for 15 min, the films were exposed for 3 h to UV irradiation (Philips HPL-N lamp, 125 W) to yield TiO_2 electrodes.

Sample Characterization. Fourier Transform Infrared studies were carried out with a Perkin-Elmer spectrum 100 FT-IR spectrophotometer using KBr pellets and a MIRacle ATR platform from PIKE Technonolgies. TGA-MS studies were performed on a Netzsch STA409 simultaneous analyzer coupled with a Thermostar GSD 300T3 Balzers Instruments mass spectrometer. Thermogravimetry (TG) curves were recorded in the 50−500 °C temperature range with a heating rate of 5 °C min^{-1} under an argon flow. The morphology of the films was investigated by field-emission scanning electron microscopy (FE-SEM) with a JEOL JSM-6700F microscope. TEM micrographs were obtained using a JEOL-JEM 2000FX microscope. The samples were prepared by a pickup from a suspension of TiO_2 nanopowder in ethanol. The texture of the TiO_2 nanoparticles and of the films scraped off the substrate was analyzed by nitrogen sorption isotherm (77 K) measurements. Data were collected using the static volumetric method with an ASAP2010 (Micromeritics) apparatus. Samples were degassed at 120 °C in

(11) Zhang, D.; Yoshida, T.; Furuta, K.; Minoura, H. *J. Photochem. Photobiol., A: Chem.* **2004**, *164*, 159.
(12) (a) Lindström, H.; Holmberg, A.; Magnusson, E.; Lindquist, S.-T.; Malmqvist, L.; Hagfeldt, A. *Nano Lett.* **2001**, *1*, 97. (b) Halme, J.; Saarinen, J.; Lund, P. *Sol. Energy Mater. Sol. Cells* **2006**, *90*, 887. (c) Yamaguchi, T.; Tobe, N.; Matsumoto, D. *Chem. Commun.* **2007**, *45*, 4767.
(13) Park, N.-G.; Kim, K. M.; Kang, M. G.; Ryu, K. S.; Chang, S. H.; Shin, Y.-Y. *Adv. Mater.* **2005**, *17*, 2349.
(14) Uchida, S.; Tomiha, M.; Takizawa, H.; Kawaraya, M. *J. Photochem. Photobiol., A: Chem.* **2004**, *164*, 93.
(15) Kim, H.; Auyeung, R.C Y.; Ollinger, M.; Kushto, G. P.; Kafafi, Z. H.; Pique, A. *Appl. Phys. A: Mater. Sci. Process.* **2006**, *83*, 73.
(16) Li, Z.; Xiao, J.; Zeng, J. *Huang Xinxing Caliao* **2006**, *34*, 56.
(17) Wang, C.-M.; Lin, S.-Y.; Chen, Y.-C. *J. Phys. Chem. Solids* **2008**, *69*, 451.
(18) De Filpo, G.; Nicoletta, F. P.; Chidichimo, G. *Chem. Mater.* **2006**, *18*, 4662.
(19) Mohmeyer, N.; Kuang, D.; Wang, P.; Schmidt, H-W.; Zakeeruddin, S. M.; Grätzel, M. *J. Mater. Chem.* **2005**, *16*, 2978.
(20) Saadeddin, I. PhD Thesis, University of Bordeaux 1, Talence, France, 2007.
(21) Zaban, A.; Aruna, S. T.; Tirosh, S.; Gregg, B. A.; Mastai, Y. *J. Phys. Chem. B* **2000**, *104*, 4130.

vacuo for a time interval long enough to reach a constant pressure (<10 μm Hg). Specific surface areas were calculated by applying the BET equation between 0.1 and 0.3 relative pressures. Pore size distributions were evaluated by the Barrett, Joyner, Halenda (BJH) method for mesopores (pores of diameter 2−50 nm).[22] The overall pore size distribution was determined using the desorption branch of the sorption isotherm and the calculation was performed by the Micromeritics software package which uses the recurrent method and applies the Harkins and Jura equation for the multilayer thickness. Powder X-ray diffraction patterns were collected on a Philips $\theta-2\theta$ PW1820 diffractometer. A continuous scan mode was used to collect 2θ data from 5−80° with a 0.1 sampling pitch and a 2° min^{-1} scan rate. Thickness determination was carried out with a KLA Tencor Alfa-step IQ profilometer.

Electrochromic Measurements. Titanium dioxide films were dried for 3 h at 120 °C under vacuum and then immersed in a lithium conducting ionic liquid electrolyte in a three-electrode configuration electrochemical cell, in a glovebox filled with argon. The electrolyte solution was composed of 0.1 M lithium bis(trifluoromethylsulfone)imide (LiTFSI) (Aldrich) in 1-butyl-3-methylimidazolium bis(trifluoromethylsulfone)imide (BMITFSI) (Solvionic). The reference electrode was a pseudo Ag/AgCl electrode and the counter electrode was a platinum plate. The electrochemical measurements were carried out with a Voltalab PGZ301 potentiostat. The UV−visible spectra were measured with an Evolution 100 spectrometer (Thermo Electron Corporation).

Results

Thin Film Preparation and Characterizations. In this work, we employed TiO_2 nanoparticles prepared by a sol−gel route followed by a hydrothermal post-treatment. TEM images revealed the formation of nanoparticles of various sizes and shapes, the average particle size being around 15 nm (Figure 1A). The as-synthesized nanoparticles were dispersed in water in the presence of a chelating agent and a nonionic surfactant to provide a stable colloidal solution. The latter was then coated over various conductive substrates by the "doctor-blade" technique and the resulting layers were illuminated under UV light to yield 1.1 μm thick films. According to SEM observations (Figure 1B), the layers were homogeneous, crack-free and composed of a porous network of aggregated nanoparticles, the size of which falls into the same range as that of the as-synthesized sol−gel particles, i.e., 15 nm. To get further insight into the actual texture and structure of the porous layers, we studied scraped off films by XRD and N_2 sorption porosimetry. The crystallinity of the UV-processed materials was similar to that of the as-prepared nanoparticles. Indeed, the anatase titanium dioxide phase was clearly identifiable in the X-ray diffraction patterns with main features at d (Å) values of {101}(3.520), {103} (2.431), {004} (2.332), {200} (1.892), {105} (1.6999), {211} (1.6665), {204} (1.4808}, {116} (1.3641), {220} (1.3378), {215} (1.2649), and {301} (1.2509).[23] The Scherrer relation was exploited, assuming a shape factor of 0.9, to estimate the average crystallite sizes using the most intense diffraction peaks.[24] An average nanocrystallite size of about 13 nm was deduced for the UV-processed films, which is in good agreement with the nanoparticle size deduced from TEM and SEM measurements. In addition, a weak peak at 30.8°, corresponding to d (Å) value of {121} (2.90 Å), revealed the presence of a small amount, i.e., 10%, of the brookite phase[25] with an average nanocrystallite size of about 8 nm. As far as the porosity of the UV-processed films is concerned, the N_2 adsorption−desorption isotherm showed a pure type IV shape with an H2 type hysteresis loop typical of mesoporous materials prepared by sol−gel or hydrothermal routes (Figure 2).[26] The pore size distribution inferred

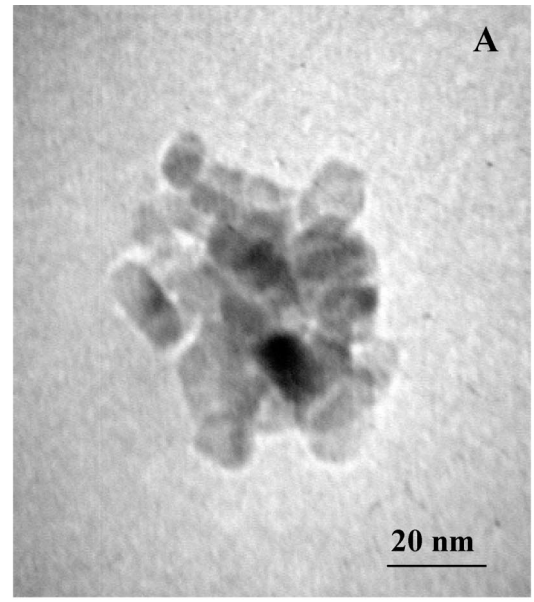

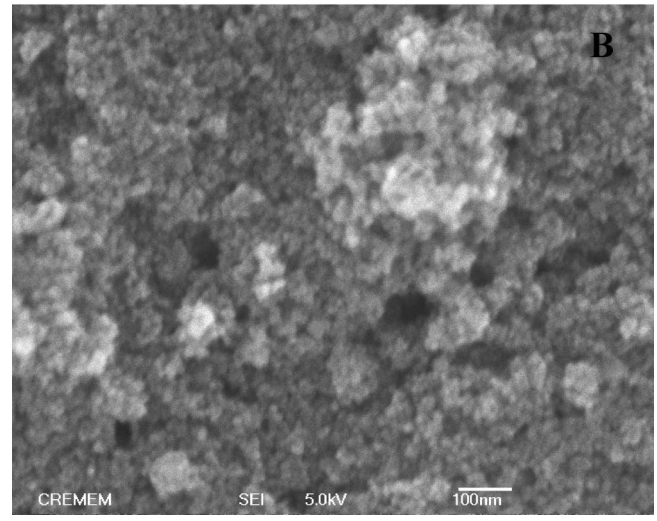

Figure 1. Texture and morphology of the TiO_2 nanoparticles and of a 1.1 μm thick UV-processed TiO_2 film. (A) TEM image of the TiO_2 Nanoparticles; (B) HR-SEM micrograph of the film.

(22) (a) Barrett, E. P.; Joyner, L.; Halenda, P. P. *J. Am. Chem. Soc.* **1951**, *73*, 373. (b) Olivier, J. P. *J. Porous Mater.* **1995**, *2*, 9.
(23) JCPDS Pattern No 21−1272 (Anatase titanium dioxide); International Center for Diffraction Data: Newtown Square, PA, 1998.
(24) The mean particle size is given by the Scherer relation $t = (0.9*\lambda)/\beta\cos\theta$ where λ is the wavelength, β the angular half-width of the *hkl* peak for the studied sample, and θ the Bragg angle for the chosen *hkl* reflection. See Eberhardt, J. P. In *Structural and Chemical Analysis of Materials*; John-Wiley & Sons: New York, 1991; p203.
(25) JCPDS Pattern No 29−1360 (Brookite titanium dioxide); International Center for Diffraction Data: Newtown Square, PA, 1998.
(26) Rouquerol, F.; Rouquerol, J.; Sing, K. In *Adsorption by Powders & Porous Solids*; Academic Press: London, 1999; p204.

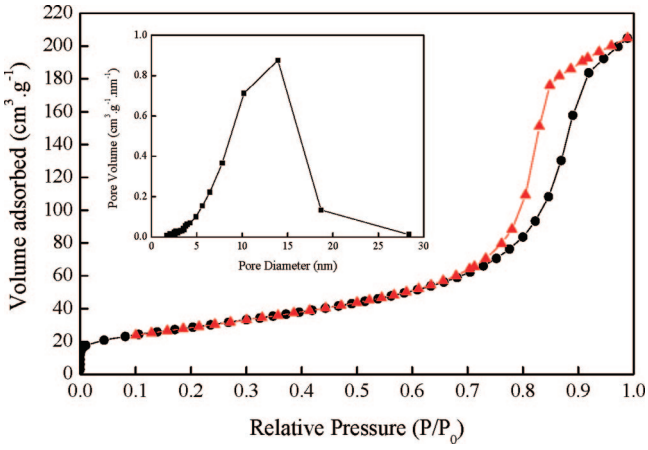

Figure 2. Nitrogen gas adsorption−desorption isotherms and pore-size distribution (inset) of a UV-processed nanoparticulate TiO_2 layer scraped off the substrate.

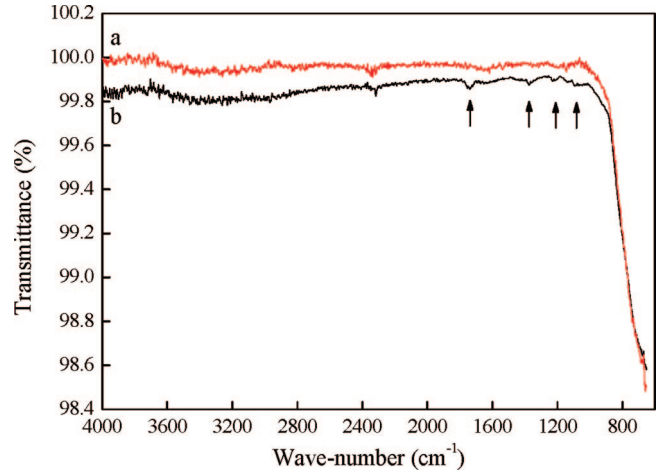

Figure 3. Infrared spectra (ATR mode) of a) the as-synthesized TiO_2 nanoparticles **1**, (b) UV-processed TiO_2 Layer. Arrows indicate the resonances mentioned in the text.

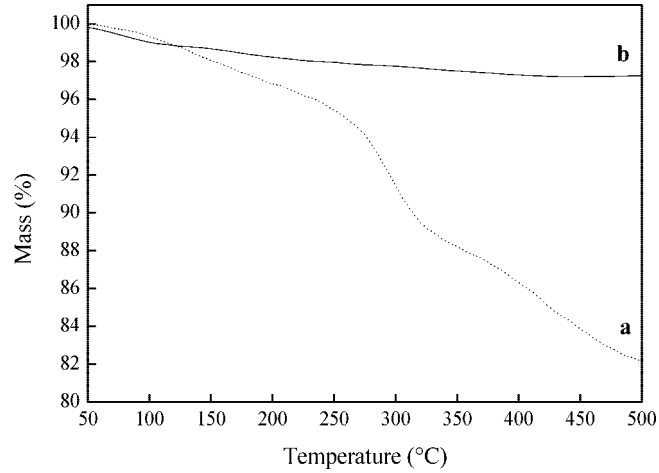

Figure 4. Thermogravimetric analysis plot of the scraped off TiO_2 films: (a) Dried in air (dotted line); (b) UV-treated in air for 3 h (full line).

from the classical BJH plot (Figure 2, inset) was rather large with an average pore size diameter of about 14 nm. Moreover, the Brunauer−Emmet−Teller (BET) specific surface area and total pore volume were estimated to be 90−100 $m^2\ g^{-1}$ and 0.34 $cm^3\ g^{-1}$, respectively, which led to an overall porosity of 55%. Consequently, these data were consistent with the formation of nanoporous anatase titania thin films exhibiting the same texture and structure as the as-prepared TiO_2 nanoparticles showing that the UV treatment has no significant densification or sintering effect.

To shed light on the nature of the organics remaining in the films after each treatment performed, scraped off films were studied by infrared spectrometry and thermogravimetry coupled to mass spectrometry (TGA-MS). Regardless the treatment used, the FTIR spectrum showed a wide absorption band due to OH stretching modes ranging from 3600 to 2500 cm^{-1} along with the associated deformation mode around 1680 cm^{-1}, a weak peak at 1380 cm^{-1} possibly related to carbonaceous species, and a prominent broad absorption bands centered at 750 cm^{-1} attributed to Ti−O and Ti−O−Ti stretching vibration modes.[27] The corresponding ATR spectra showed the presence of a broad peak below 650 cm^{-1} corresponding to TiO_2 lattice vibrations, and two broad peaks around 1600 cm^{-1} and 3200 cm^{-1} corresponding to water and hydroxyl groups. Nonetheless, the UV-processed film showed weak peaks at 1738, 1374, 1227, and around 1100 cm^{-1}; which might be attributed to the presence of small amounts of carbonates (Figure 3).[28] Furthermore, the TG (thermogravimetric) curves shown in Figure 4 depict the change in the mass of the films, dried at RT or UV-exposed in air for 3 h after drying, between 50 and 500 °C under an argon flow. The TG of the dried films (Figure 4A) showed a continuous mass loss occurring in three main successive steps of 3.8% (from 50 to 200 °C), 8.4% (from 200 to 420 °C) and 6.0% (from 420 to 500 °C) to yield a final residue of 81.8%. The main species detected by MS measurements were water (*m*/*z* 18), carbon dioxide (*m*/*z* 22, 44), ethanol and its fragments (*m*/*z* 29, 45, 46), pentan-2,4-dione and its fragments (*m*/*z* 43, 58, 60 99) and fragments of Triton X as benzene (*m*/*z* 50, 51, 52, 76, 77, 78) and octyl chains (97, 112). According to the molecular ion fragment trends as function of the temperature,[29] the three pyrolysis steps can be rationalized as follows: (i) removal of physisorbed water and pentan-2,4-dione; (ii) loss of structural water along with the thermal decomposition of Triton-X and coordinated pentan-2,4-dionato species via retro-Claisen reactions;[30] (iii) elimination of residual Triton-X fragments and of remaining carbon as carbon dioxide.

By contrast, the TG of the UV-treated films (Figure 4B) showed a slight total mass loss of about 2.8% taking place in three steps of 1.2% (from 50 to 140 °C), 0.8% (from 140 to 230 °C), and 0.8% (from 230 to 500 °C), which was on the same order of magnitude as one of the as-synthesized nanoparticles. Moreover, no fragments characteristic of the pentan-2,-4-dione or Triton-X were detected by mass spectrometry. As a result, all these data show the almost complete

(27) Farmer, G. E., Ed.; *The Infrared Spectra of Minerals*; Mineral Society: London, 1974.
(28) Connor, P. A.; Dobson, K. D.; McQuillan, A. J. *Langmuir* **1999**, *15*, 2402.
(29) See the Supporting Information.
(30) (a) Poncelet, O.; Hubert-Pflalzgrah, L. G. *Polyhedron* **1990**, *9*, 1305. (b) Gamard, A.; Babot, O.; Jousseaume, B.; Rascle, M.-C.; Toupance, T.; Campet, G *Chem. Mater.* **2000**, *12*, 3419.

UV-removal of the organic chelating agent and surfactant, the only remaining carbon traces existing as carbonates at the surface of the TiO_2 nanoparticles.

Electrochromic Properties of the UV-Processed TiO_2 Films. Anatase TiO_2 is able to insert small ions in organic medium such as lithium according to the following reaction[31]

$$Ti^{4+}O_2 + xLi^+ + xe^- \rightarrow Li_xTi^{4+}_{1-x}Ti^{3+}_xO_2 \qquad (1)$$

The $3d^1$ (Ti^{3+}) energy levels resulting from the reduction of some Ti^{4+} into Ti^{3+} as depicted in (1) give rise to electronic transitions from the $3d^1$ (Ti^{3+}) sub-band gap states to the $3d^0$(Ti^{4+}) character conduction band which induces the blue color of the titania layer. All of the experiments were performed between −1.55 and 0.00 V vs Ag/AgCl in order to achieve maximum coloration and at the same time prevent any degradation due to irreversible insertion into the ITO conductive substrate.

The coloration/decoloration of the UV-processed TiO_2 films substrates was studied by monitoring the optical absorbance in the course of the Li insertion/extraction by UV−visible spectrophotometry in the wavelength range 350−1100 nm. The coloration efficiency is the most relevant parameter describing the performances of electrochromic devices. It is defined as the change in optical density per unit of inserted charge per unit of area and has been calculated according to the following equation

$$CE = (\Delta OD)/\Delta Q$$

where ΔOD is the difference of optical density between the bleached and the colored states, and ΔQ (C cm^{-2}) is the injected electronic charge responsible for the optical change.

The electrochromic behavior of the nanoporous TiO_2 UV-processed layers was first evidenced on FTO/glass transparent conductive substrates. The 1.1 μm-thick films effectively inserted lithium ions in the LiTFSI/BMITFSI electrolyte as they underwent 30 s−30 s chronoamperometric cycles. The capacity slightly decreased from 18 to 16 mC cm^{-2} after 2000 cycles (Figure 5A), which was confirmed by the cyclic voltammograms recorded in LiTFSI/BMITFSI electrolyte after 1000 and 2000 chronoamperometric cycles (Figure 5B). The current remained close to zero up to a threshold voltage, beyond which it increased rapidly. The reduction peak was broad and exhibited a maximum centered at −1.45 V vs Ag/AgCl. Upon reversal of the potential scan, the inserted lithium ions were extracted and the corresponding oxidation current wave was also broad and was centered at −1.0 V vs Ag/AgCl. At the end of the back and forth scans, the film was completely bleached, indicating the excellent reversibility of the intercalation process. These UV-processed films were therefore stable up to 2000 cycles. Nonetheless, the insertion process was not finished after 30 s as indicated by the nonzero reduction current (Figure 5A, inset). The measurements were therefore reproduced by using longer 2 min - 1 min chronoamperometric cycles to achieve maximum coloration.[29] There is a 10% decrease in capacity over 300 cycles with a cyclic voltammogram similar to that of the film that underwent 2000 cycles. The optical and coloration efficiency spectra indicated that a good 1.1 optical change

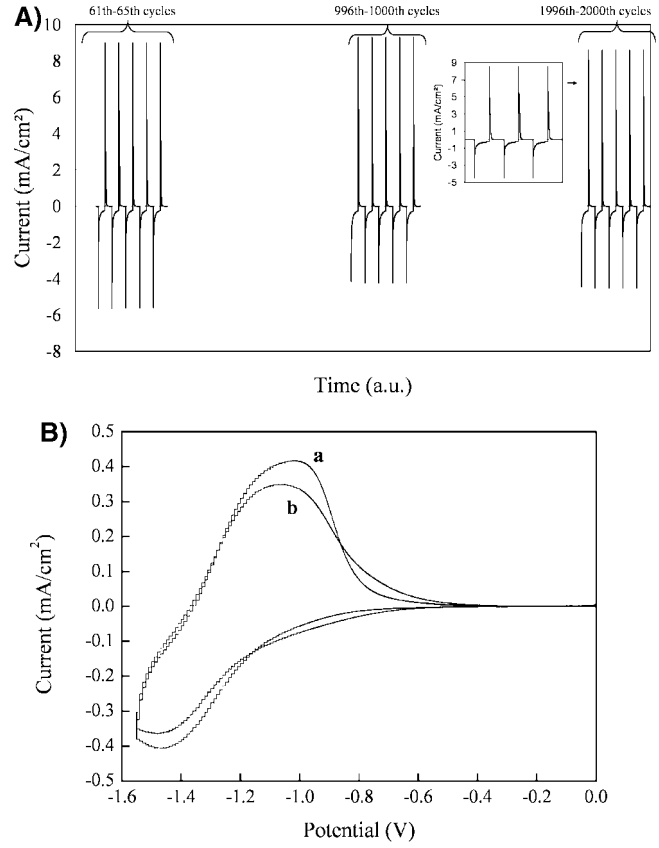

Figure 5. Electrochromic response of a UV-processed, 1.1 μm thick TiO_2 film deposited on FTO glass.

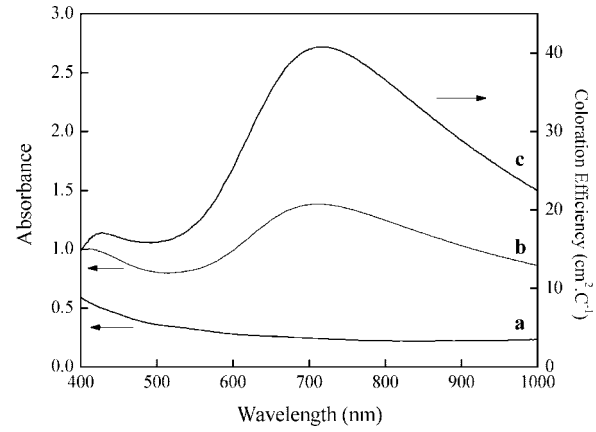

Figure 6. UV−visible spectra of a UV-processed 1.1 μm thick TiO_2 film deposited on FTO/glass (a) in the bleached state; (b) in the colored state; (c) the corresponding coloration efficiency.

(ΔOD) was observed at 710 nm for a capacity of ∼28 mC cm^{-2}, leading to a coloration efficiency of 40 cm^2 C^{-1} at 710 nm and 18.4 cm^2 C^{-1} at 550 nm (Figure 6).

The measurements were then extended to UV-processed TiO_2 layers deposited on flexible substrates such as ITO/PET. The cyclic voltammogram of such films showed a large ohmic drop compared to FTO/glass supported systems because the reduction step occurred below −1.55 V vs Ag/AgCl (Figure 7B), and the oxidation one around −0.60 V vs Ag/AgCl to be compared with −1.5 V vs Ag/AgCl and −1.0 V vs Ag/AgCl found with rigid substrates. However, upon cycling for 300 cycles between −1.55 and 0.00 V vs Ag/AgCl, the capacity slightly decreased of 6%, from 17 to

(31) Wang, C. M.; Lin, S. Y. *J. Solid-State Electrochem.* **2006**, *10*, 255.

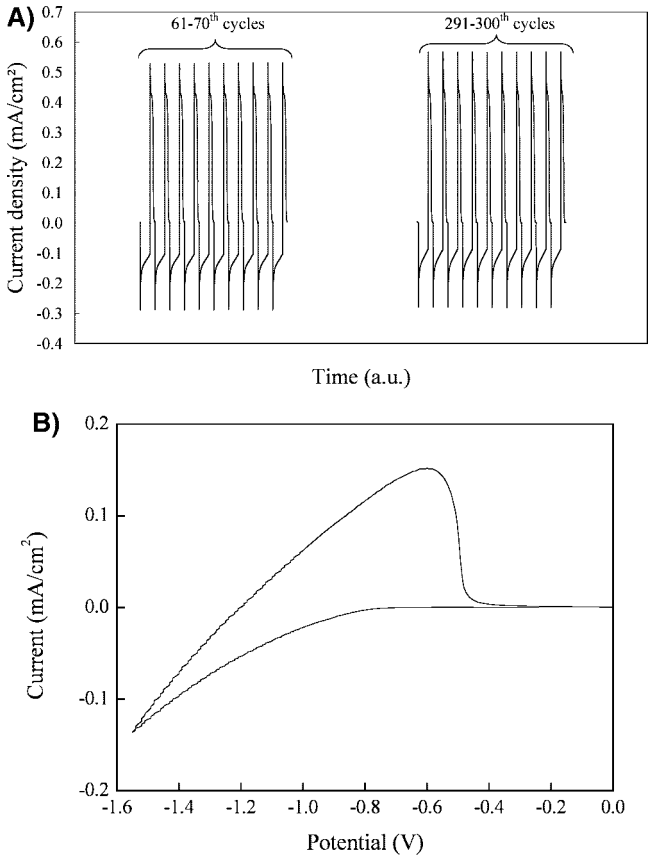

Figure 7. Electrochromic response of a UV-processed 1.1 μm thick TiO_2 film deposited on ITO/PET; (A) chronoamperometric cycles (30 s−30 s); (B) Cyclic voltammograms (scan rate: 10 mV s^{-1}) after 300 cycles.

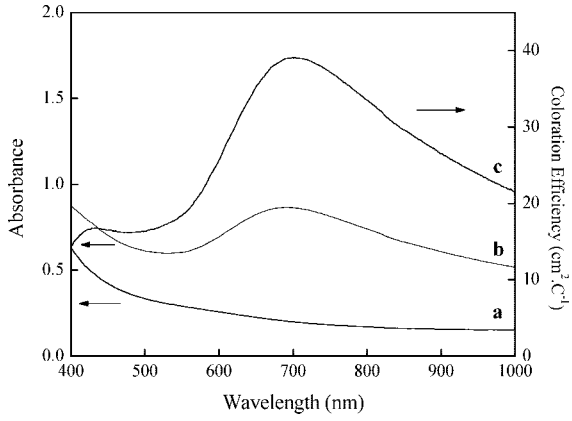

Figure 8. UV−visible spectra of a UV-processed 1.1 μm thick TiO_2 film deposited on ITO/PET (a) in the bleached state; (b) in the colored state; (c) the corresponding coloration efficiency.

16 mC cm^{-2} (Figure 7A). Furthermore, the optical difference between the bleached and the colored films (17 mC cm^{-2}) was 0.65 at 710 nm, which corresponds to a coloration efficiency of 38 cm^2 C^{-1} (Figure 8).

To circumvent the limitation due to the rather high resistance of the ITO/PET substrate, a gold layer was sputtered on the top of such a surface to provide sheet resistance as low as 15 Ω/□. The cyclic voltammogram of UV-processed TiO_2 films coated on the resulting conductive substrate showed that the reduction peak was around −1.50 V vs Ag/AgCl and that the oxidation one was located around −0.90 V vs Ag/AgCl indicating a decrease of the ohmic drop compared to the films on ITO/PET.[29] However, after 300 cycles, some parts of the film became inactive and the capacity decreased from 29 to 18 mC cm^{-2}. This phenomenon can be rationalized by postulating a poorly controlled gold/TiO_2 interface, since the film was damaged much more than when it was coated over the ITO or FTO substrates.

Table 1. Response Time for Coloration (T_c) and Bleaching (T_b), Optical Modulations at 550 nm (ΔOD_{550}) and 710 nm (ΔOD_{710}), and Coloration Efficiencies at 550 nm (CE_{550}) and 710 nm (CE_{710})

sample	T_c (s)	T_b (s)	ΔOD_{550}	CE_{550} (cm^2 C^{-1})	ΔOD_{710}	CE_{710} (cm^2 C^{-1})
TiO_2 film on FTO glass	69	7	0.5 (33%)	18	1.1	40
TiO_2 film on ITO/PET	97	31	0.3 (26%)	18	0.7	38

Discussion

This study shows that a direct UV treatment in air of a nanoparticulate TiO_2 film is sufficient to induce the interconnection of the nanoparticles with the complete removal of the organics used during the deposition process. The question regarding the chemical process leading to the nanoparticle interconnection and the film formation therefore arises. First of all, the almost complete removal of the organics present in the starting colloid can be related to the photocatalytic activity of titania under UV irradiation.[32] Furthermore, several works have shown the UV irradiation of titania induces highly hydrophilic surfaces.[33] Various mechanisms have been proposed to explain this enhancement of hydrophilicity including UV-induced defect production,[34] UV-induced rupture of Ti−OH bonding[33d] or photo-oxidation of hydrophobic contaminant layers,[35] the main differences between these studies lye in the experimental conditions used. Even though the exact origin of such a behavior still remains a topic of debate, the interparticle connection under UV irradiation can be rationalized as follows. First of all, ozone molecules, formed by UV irradiation in air, react with water adsorbed on the TiO_2 surface or present in the air to yield hydrogen peroxide. Decomposition of the latter in the presence of water then provides −OH or −OOH radicals, which can be trapped by Ti^{3+} sites to give surface hydroxyl groups. Another possibility is the dissociation of water molecules adsorbed on defect sites created by UV irradiation to form singly or doubly coordinated surface hydroxyls. The further condensation of these groups through oxolation reactions then leads to the particle interconnection. One has to emphasis that such a process has been previously

(32) Hoffmann, M. R.; Martin, S. T.; Choi, W.; Bahnemann, D. W. *Chem. Rev.* **1995**, *95*, 69.
(33) (a) Miyauchi, M.; Nakajima, A.; Fujishima, A.; Hashimoto, K.; Watanabe, T. *Chem. Mater.* **2000**, *12*, 3. (b) Sakai, N.; Fujishima, A.; Watanabe, T.; Hashimoto, K. *J. Phys. Chem. B* **2001**, *105*, 3023. (c) Stevens, N.; Priest, C. I.; Sedev, R.; Ralston, J. *Langmuir* **2003**, *19*, 3272. (d) Gao, Y.; Masuda, Y.; Koumoto, K. *Langmuir* **2004**, *20*, 3188.
(34) Wang, R.; Hashimoto, K.; Fujishima, A.; Chikuni, M.; Kojima, E.; Kitamura, A.; Shimohigoshi, M; Watanabe, T. *Adv. Mater.* **1998**, *10*, 135.
(35) Thompson, T. L.; Yates, J. T. *Chem. Rev.* **2006**, *106*, 4428.

evidenced for silica.[36] Thus, it has been shown that UV irradiation of ordered nanocomposite silica thin films removes the organic templating phase and condenses silica. Furthermore, in this work, this route leads to conductive TiO_2 layers made of a porous network of aggregated nanoparticles with an average pore size of about 14 nm. According to the IUPAC classification,[37] these films are clearly mesoporous, the mesoporosity arising from the interparticle space.

The performances of these UV-processed films are gathered in Table 1. The TiO_2 films coated over various substrates showed good electrochromic responses with close behaviors and coloration efficiencies. The nanoporous and nanoparticulate UV-processed films are therefore good candidates for electrochromic applications because of their large electrochemically active surface area which enables fast response, good reversibility, and a large insertion rate of lithium ions.[38]

Nonetheless, the films on an ITO/PET substrate insert less lithium over the same time (17 compared to 30 mC cm^{-2} in 2 min), probably because of a slower insertion rate, the reduction peak being shifted to more negative potentials on ITO/PET because of the higher sheet resistance of the ITO/PET ($R_\square = 70\ \Omega$) compared to that of FTO/glass ($R_\square = 10\ \Omega$). To circumvent this limitation, sputtering gold on the ITO to increase the conductivity was performed. The films effectively insert approximately the same amount of lithium over 2 min, i.e., 31 versus 29 mC cm^{-2} for films on FTO/glass and Au/ITO/PET, respectively. The issue regarding Au/TiO_2 interface stability should be solved by sputtering another layer of ITO on the top of the gold layer.

Regardless of the film studied, insertion and desinsertion of Li^+ in the TiO_2 films do not show identical profiles. A first explanation may be the fact that the insertion is governed by the properties at the boundary between the electrolyte and the titanium oxide film whereas desinsertion is only ruled by ion transport in the film.[38] Another reason results from the fact that if the oxidation voltage is located far beyond the oxidation peak potential of the film, in the reduction case, to avoid the TCO degradation the applied voltage is very close to the film reduction potential. Furthermore, the integration shows a 10% decrease in the film capacity with time, which could be due to a slight loss of mechanical stability upon extended cycling in the liquid electrolyte. This issue could be solved by making devices with a quasi-solid electrolyte, for instance by blending the ionic liquid with poly(methyl methacrylate).[39,40]

Finally, Table 2 gives an overview of the TiO_2 electrochromic systems described in the literature. All the films were deposited on transparent conductive oxide/glass substrates. These films were mainly made through high-temperature techniques (one at 150 °C) and sintering temperatures as high as 560 °C. Therefore, the UV-processed TiO_2 films described here are the first room temperature ones exhibiting such high coloration efficiencies. An additional crucial point concerns the long-term cycling of these layers which even after 2000 cycles still exhibit high coloration efficiencies, such long-term behavior being unknown in the literature. In addition, these performances are reached in a nonconventional medium based on ionic liquid, which is more viscous than the classical electrolyte.

Table 2. Comparison of the Electrochromic Performances of the High Temperature Processed Films Described in the Literature with those of the UV-processed Films Described in this Work (ΔOD, Optical Modulation; CE, Coloration Efficiency)

reference	film thickness (μm)	wavelength (nm)	ΔOD (ΔT)	CE ($cm^2\ C^{-1}$)	capacity ($mC\ cm^{-2}$)
41	0.4	630	(10.5%)	4.3	2.45
42	0.6	550	(32.4%)	6.1	6.5
		550	(42%)	8.1	6.4
		700		17	6.4
43	[a]	550	(49.5%)	11.4	7.6
31	0.164	550	0.13	4.5	28.2
44	[a]	630		20	6.7
38	0.135	633	<0.15	13	12.5
17	0.3	550	0.27	24.5	11
45	0.35	550	0.087(14.2%)	7.98	10.9
this work on FTO glass	1.1	550	0.5(33%)	18	28
		630	0.9(53%)	32	28
		710	1.2(54%)	40	28
this work on ITO/PET	1.1	550	0.3(26%)	18	17
		630	0.5(41%)	32	17
		710	0.7(50%)	38	17

[a] Not precise.

Conclusion

A low-temperature processing of TiO_2 films by UV irradiation was successfully developed to yield nanoporous and nanocrystalline anatase layers on various kinds of substrates. These films show good electrochromic responses and high coloration efficiencies in an ionic liquid, which is a stable and environmental friendly solvent (nonflammable, nonvolatile). The coloration efficiency reaches 38 $cm^2\ C^{-1}$ for films on ITO/plastic, for a 0.65 absorption change at 710 nm whereas the corresponding film on FTO/glass shows a 40 $cm^2\ C^{-1}$ coloration efficiency for a 1.1 absorbance change at 710 nm. The nanoparticulate structure and high specific surface area (>90 $m^2\ g^{-1}$) of these films provide a large number of insertion sites, and the high surface-to-volume ratio ensures minimal diffusion path lengths. Compared to bulk materials, such a three-dimensional network of nanoparticles has a much larger tolerance for the mechanical stress that occurs during the insertion−desinsertion processes.

This method should be easily extended to the preparation of other electrochromic metal oxides as NiO or MnO_2. Efforts

(36) (a) Dattelbaum, A. M.; Amweg, M. L.; Ruiz, J. D.; Ecke, L. E.; Shreve, A. P.; Parikh, A. N. *J. Phys Chem. B* **2005**, *109*, 14551. (b) Sanchez, C.; Boissière, C.; Grosso, D.; Laberty, C.; Nicole, L. *Chem. Mater.* **2008**, *20*, 682.
(37) Sing, K. S. W.; Everett, D. H.; Haul, R.A.W.; Moscou, L.; Pierotti, R. A.; Rouquerol, J.; Siemieniewska, T *Pure Appl. Chem.* **1985**, *57*, 603.
(38) van de Kron, R.; Goosens, A.; Schoonman, J. *J. Phys. Chem. B* **1999**, *103*, 7151.
(39) Campet, G.; Mingotaud, C., Poquet, A. International Patent, WO 052338, 2001.
(40) Duluard, S.; Grondin, J.; Bruneel, J-L.; Campet, G.; Delville, M-H.; Lassègues, J-L. *J. Raman Spectrosc.* **2008**, *39*, 1189.
(41) Shinde, P. S.; Deshmukhb, H. P.; Mujawar, S. H.; Inamdar, A. I.; Patil, P. S. *Electrochim. Acta* **2007**, *52*, 3114.
(42) Verma, A.; Agnihotry, S. A. *Electrochim. Acta* **2007**, *52*, 2701.
(43) Verma, A.; Basu, A.; Bakhshi, A. K.; Agnihotry, S. A. *Solid State Ionics* **2005**, *176*, 2285.
(44) Vuk, S.; Jese, R.; Gaberscek, M.; Orel, B.; Drazic, G. *Sol. Energy Mater. Sol. Cells* **2006**, *90*, 452.
(45) Lin, S-Y.; Chen, Y-C.; Wang, C-M.; Liu, C-C. *J. Solid-State Electrochem.* **2008**, *12*, 1481.

are currently in progress in this direction along with the decrease of the film thickness and the corresponding findings will be presented very soon.

Acknowledgment. Elisabeth Sellier (CREMEM, University of Bordeaux) is acknowledged for her precious assistance. The authors thank the CNRS, the Aquitaine Region (ZT PhD fellowship), Du Pont (USA), and the European Community (FAME network of Excellence) for partial support of this work.

Supporting Information Available: FTIR spectra of the as-synthesized TiO_2 nanoparticles, of scraped off UV-processed or calcined TiO_2 layers, TGA-MS traces of scraped off UV-processed films, chronoamperometric responses, and cyclic voltammograms of UV-processed TiO_2 films deposited onto FTO/glass and Au-ITO-PET substrates (PDF). This material is available free of charge via the Internet at http://pubs.acs.org.

CM802030C